Inorg. Chem. **2008**, *47*, 8674−8686

Investigation of Layered Double Hydroxides Intercalated by Oxomolybdenum Catecholate Complexes

Bernardo Monteiro,[†] Sandra Gago,[†] Filipe A. Almeida Paz,[†] Robert Bilsborrow,[‡] Isabel S. Gonçalves,[†] and Martyn Pillinger*[,†]

Department of Chemistry, CICECO, University of Aveiro, 3810-193 Aveiro, Portugal, and CCLRC Daresbury Laboratory, Warrington, Cheshire WA4 4AD, U.K.

Received March 7, 2008

Oxomolybdenum(VI) complexes of 3,4-dihydroxybenzoic acid (3,4-H_2dhb) have been incorporated into layered double hydroxides (LDHs) by treatment of the LDH−nitrate (Zn−Al, Mg−Al) or LDH−chloride (Li−Al) precursors with aqueous or water/ethanol solutions of the complex $(NMe_4)_2[MoO_2(3,4\text{-dhb})_2]\cdot 2H_2O$ at 50 or 100 °C. The texture and chemical composition of the products were investigated by elemental analysis and scanning electron microscopy (SEM) with coupled energy dispersive spectroscopy (EDS). Microanalysis for N and EDS analysis for Cl showed that at least 90% of nitrate or chloride ions were replaced during the ion exchange reactions. The final Mo content in the materials varied between 6.5 and 11.6 wt %. Mo K-edge EXAFS analysis, supported by IR, Raman, UV−vis, and $^{13}C\{^1H\}$ CP/MAS NMR spectroscopic studies, showed the presence of cointercalated $[MoO_2(3,4\text{-dhb})_2]^{m-}$ and $[Mo_2O_5(3,4\text{-dhb})_2]^{m-}$ complexes in proportions that depend on the type of LDH support and the reaction conditions. The binuclear bis(catecholate) complex, with a Mo···Mo separation of 3.16 Å, was the major species intercalated in the Zn−Al and Li−Al products prepared using only water as solvent. The X-ray powder diffraction (XRPD) patterns of all the Mo-containing LDHs showed the formation of an expanded phase with a basal spacing around 15.4 Å. High-resolution synchrotron XRPD patterns were indexed with hexagonal unit cells with a *c*-axis of either 30.7 (for Li−Al−Mo LDHs) or 45.9 Å (for a Zn−Al−Mo LDH). Fourier maps (F_{obs}) calculated from the integrated intensities extracted from Le Bail profile decompositions indicated that the binuclear guest species are positioned such that the Mo → Mo vector is parallel to the host layers, and the overall orientation of the complex is perpendicular to the same layers. The thermal behavior of selected materials was studied by variable-temperature XRPD, thermogravimetric analysis (TGA), and differential scanning calorimetry (DSC).

Introduction

Only a few families of inorganic layered compounds with positively charged layers compensated by intercalated anions are known.[1] By far the most studied group are layered double hydroxides (LDHs), also known as anionic clays or hydrotalcite-like compounds (because of the mineral with the formula $Mg_6Al_2(OH)_{16}CO_3\cdot 4H_2O$). The structure of LDHs can be considered as derived from that of brucite, $Mg(OH)_2$, by replacement of some of the Mg^{2+} cations in the $Mg(OH)_2$ sheets by M^{3+} cations, electric balance being achieved through insertion of anions into the interlayer region, where water molecules also reside. The sheets may stack with either hexagonal or rhombohedral symmetry. Among the various synthesis methods available for LDHs,[1a,2] the most common involves coprecipitation of the component hydroxides with precise control of pH. The general formula of the resultant materials can be written as $[M^{2+}_{1-x}M^{3+}_x(OH)_2](X^{n-})_{x/n}\cdot zH_2O$

* To whom correspondence should be addressed. E-mail: mpillinger@ua.pt.
† University of Aveiro.
‡ CCLRC Daresbury Laboratory.

(1) (a) *Layered Double Hydroxides: Present and Future*; Rives, V., Ed.; Nova Science Publishers, Inc.: New York, 2001. (b) Williams, G. R.; O'Hare, D. *J. Mater. Chem.* **2006**, *16*, 3065. (c) Fogg, A. M.; Williams, G. R.; Chester, R.; O'Hare, D. *J. Mater. Chem.* **2004**, *14*, 2369. (d) Rojas, R.; Barriga, C.; Ulibarri, M. A.; Malet, P.; Rives, V. *J. Mater. Chem.* **2002**, *12*, 1071. (e) Kandare, E.; Hossenlopp, J. M. *Inorg. Chem.* **2006**, *45*, 3766. (f) Gándara, F.; Perles, J.; Snejko, N.; Iglesias, M.; Gómez-Lor, B.; Gutiérrez-Puebla, E.; Monge, M. Á. *Angew. Chem.* **2006**, *118*, 8166.

(2) Evans, D. G.; Duan, X. *Chem. Commun.* **2006**, 485.

(3) (a) Besserguenev, A. V.; Fogg, A. M.; Francis, R. J.; Price, S. J.; O'Hare, D.; Isupov, V. P.; Tolochko, B. P. *Chem. Mater.* **1997**, *9*, 241. (b) Fogg, A. M.; Freij, A. J.; Parkinson, G. M. *Chem. Mater.* **2002**, *14*, 232.

10.1021/ic800420a CCC: $40.75
Published on Web 08/26/2008

(X = anion). In addition to these materials with +2 and +3 metal cations in different ratios, there is a unique subset containing +1 and +3 cations, namely, the Li−Al−X LDHs with the general formula $[LiAl_2(OH)_6](X^{n-})_{1/n}\cdot zH_2O$.[3a] The hexagonal Li−Al−X LDH system is prepared by filling of octahedral holes in the layers of gibbsite [γ-$Al(OH)_3$] with Li^+ through direct reaction with LiX salts and displays cation ordering within the layers. Rhombohedral Li−Al LDHs can also be prepared through the intercalation of the other $Al(OH)_3$ polymorphs bayerite and nordstrandite.[3b]

LDHs exhibit a rich intercalation chemistry because the charge-balancing anions can be replaced by other species through an ion exchange process.[4] Although the bulk of the research has centered on the intercalation of organic and inorganic anions, the intercalation of metallo-organic anions has also attracted considerable interest because the properties of the guests in the resultant nanostructured hybrid materials are often different from those of the bulk compound. LDHs containing metal complexes of the organic ligands oxalate,[5] EDTA,[6] citrate,[7] nitrilotriacetate,[8] salens,[9] phthalocyanines,[10] porphyrins,[10b,11] and triphenyl phosphine derivatives[12] have been prepared, either directly by intercalation of the metal complex or indirectly by forming the metal complex between the host layers, following intercalation of the ligand. Several of these materials show potential as heterogeneous catalysts for organic transformations, such as the hydrogenation, hydroformylation, and epoxidation of olefins. Another interesting class of guests for LDHs are oxometal complexes.[13] For example, dioxomolybdenum(VI) complexes are important catalysts or catalyst precursors for oxygen-atom transfer reactions in chemical and biological systems.[14] Corma and co-workers reported the intercalation of the anion $[MoO_2(O_2CC(S)Ph_2)_2]^{2-}$ into the interlamellar space of a Zn−Al LDH and its application as a catalyst for the oxidation of thiols by molecular oxygen.[13a]

We recently described the incorporation of an oxomolybdenum complex of 3,4-dihydroxybenzoic acid (3,4-H_2dhb) into Zn−Al LDHs by ion-exchange reactions with precursor materials in nitrate form.[13d] The present paper describes the expansion of this work, with the synthesis and characterization of Zn−Al, Mg−Al, and Li−Al LDHs intercalated by oxomolybdenum complexes of 3,4-H_2dhb. The Li−Al system was chosen because the materials in this family of LDHs are typically highly crystalline, and we anticipated that analysis of the synchrotron X-ray powder diffraction patterns of the resultant intercalates could yield useful information about the organization of the guests in the interlayers. In combination with several other methods, such as IR spectroscopy and EXAFS, it is shown that dimerization of the monomeric precursor complex occurs during contact with the LDH supports, resulting in the intercalation of oxo-bridged catecholate complexes.

Experimental Section

Materials. The starting materials gibbsite [γ-$Al(OH)_3$] (Merck), LiCl, $Mg(NO_3)_2\cdot 6H_2O$, $Zn(NO_3)_2\cdot 6H_2O$ (Riedel de Haën), $Al(NO_3)_3\cdot 9H_2O$ (Riedel de Haën), 50% aqueous NaOH (Aldrich), molybdic acid ($MoO_3\cdot nH_2O$), and tetramethylammonium hydroxide pentahydrate were obtained from commercial sources and used as received. The complexes $[MoO_2Cl_2(DMF)_2]$[15] and $(NMe_4)_2[MoO_2$-(3,4-dhb)$_2]\cdot 2H_2O$ (**1**)[13d] were prepared as described previously.

Zn−Al−NO_3 LDH. The Zn−Al layered precursor containing nitrate anions with a Zn/Al molar ratio of ~1.9 was prepared as described previously by addition of a mixed solution of $Zn(NO_3)_2$ and $Al(NO_3)_3$ to a solution containing $NaNO_3$ and NaOH, followed by aging of the precipitate at 85 °C for 18 h.[13d] Anal. Calcd for $[Zn_{3.86}Al_2(OH)_{11.72}](NO_3)_{1.7}(CO_3)_{0.15}\cdot 3H_2O$: Zn, 37.44; Al, 8.00; C, 0.27; H, 2.65; N, 3.53. Found: Zn, 37.48; Al, 8.03; C, 0.25; H, 2.46; N, 3.53%. IR (cm^{-1}): 3472br, 1617br, 1431sh, 1383vs, 826w, 681s,bd, 615m, 558sh, 425vs, 316m. Raman (cm^{-1}): 1400w, 1055vs, 717w, 551m, 488w, 255w, 206w.

Mg−Al−NO_3 LDH. A solution (100 mL) of $Mg(NO_3)_2$ and $Al(NO_3)_3$ (Mg^{2+} = 0.50 M, Al^{3+} = 0.25 M) in deionized and decarbonated (DD) water was added under nitrogen to DD water (150 mL) using a Metrohm 776 Dosimat. The pH of the mixture

(4) (a) Khan, A. I.; O'Hare, D. *J. Mater. Chem.* **2002**, *12*, 3191. (b) Newman, S. P.; Jones, W. *New J. Chem.* **1998**, *22*, 105. (c) Leroux, F.; Taviot-Guého, C. *J. Mater. Chem.* **2005**, *15*, 3628. (d) Rives, V.; Ulibarri, M. A. *Coord. Chem. Rev.* **1999**, *181*, 61.

(5) (a) del Arco, M.; Gutiérrez, S.; Martín, C.; Rives, V. *Inorg. Chem.* **2003**, *42*, 4232. (b) Coronado, E.; Galán-Mascarós, J. R.; Martí-Gastaldo, C.; Ribera, A. *Chem. Mater.* **2006**, *18*, 6112. (c) Prevot, V.; Forano, C.; Besse, J. P. *J. Solid State Chem.* **2000**, *153*, 301.

(6) (a) Wu, G.; Wang, L.; Yang, L.; Yang, J. *Eur. J. Inorg. Chem.* **2007**, 799. (b) Tsyganok, A.; Green, R. G.; Giorgi, J. B.; Sayari, A. *Catal. Commun.* **2007**, *8*, 2186. (c) Pérez, M. R.; Pavlovic, I.; Barriga, C.; Cornejo, J.; Hermosín, M. C.; Ulibarri, M. A. *Appl. Clay Sci.* **2006**, *32*, 245. (d) Li, C.; Wang, G.; Evans, D. G.; Duan, X. *J. Solid State Chem.* **2004**, *177*, 4569. (e) Tarasov, K. A.; O'Hare, D.; Isupov, V. P. *Inorg. Chem.* **2003**, *42*, 1919.

(7) (a) Wang, L.-Y.; Wu, G.-Q.; Evans, D. G. *Mater. Chem. Phys.* **2007**, *104*, 133. (b) Wu, G.; Wang, L.; Evans, D. G.; Duan, X. *Eur. J. Inorg. Chem.* **2006**, 3185.

(8) (a) Gutmann, N. H.; Spiccia, L.; Turney, T. W. *J. Mater. Chem.* **2000**, *10*, 1219. (b) Kaneyoshi, M.; Jones, W. *Mol. Cryst. Liq. Cryst.* **2001**, *356*, 459. (c) Kaneyoshi, M.; Jones, W. *J. Mater. Chem.* **1999**, *9*, 805.

(9) (a) Bhattacharjee, S.; Anderson, J. A. *Chem. Commun.* **2004**, 554. (b) Bhattacharjee, S.; Anderson, J. A. *J. Mol. Catal. A: Chem.* **2006**, *249*, 103. (c) Choudary, B. M.; Ramani, T.; Maheswaran, H.; Prashant, L.; Ranganath, K. V. S.; Kumar, K. V. *Adv. Synth. Catal.* **2006**, *348*, 493.

(10) (a) Carrado, K. A.; Forman, J. E.; Botto, R. E.; Winans, R. E. *Chem. Mater.* **1993**, *5*, 472. (b) Ukrainczyk, L.; Chibwe, M.; Pinnavaia, T. J.; Boyd, S. A. *J. Phys. Chem.* **1994**, *98*, 2668. (c) Barbosa, C. A. S.; Ferreira, A. M. D. C.; Constantino, V. R. L.; Coelho, A. C. V. *J. Incl. Phenom. Macro. Chem.* **2002**, *42*, 15. (d) Xiong, Z.; Xu, Y. *Chem. Mater.* **2007**, *19*, 1452.

(11) (a) Halma, M.; Wypych, F.; Drechsel, S. M.; Nakagaki, S. *J. Porphyrins Phthalocyanines* **2002**, *6*, 502. (b) Barbosa, C. A. S.; Ferreira, A. M. D. C.; Constantino, V. R. L. *Eur. J. Inorg. Chem.* **2005**, 1577. (c) Lang, K.; Bezdička, P.; Bourdelande, J. L.; Hernando, J.; Jirka, I.; Káfuňková, E.; Kovanda, F.; Kubát, P.; Mosinger, J.; Wagnerová, D. M. *Chem. Mater.* **2007**, *19*, 3822.

(12) (a) Iosif, F.; Parvulescu, V. I.; Pérez-Bernal, M. E.; Ruano-Casero, R. J.; Rives, V.; Kranjc, K.; Polanc, S.; Kočevar, M.; Genin, E.; Genêt, J-P.; Michelet, V. *J. Mol. Catal. A: Chem.* **2007**, *276*, 34. (b) Wei, M.; Zhang, X.; Evans, D. G.; Duan, X.; Li, X.; Chen, H. *AIChE J.* **2007**, *53*, 2916.

(13) (a) Cervilla, A.; Corma, A.; Fornés, V.; Llopis, E.; Palanca, P.; Rey, F.; Ribera, A. *J. Am. Chem. Soc.* **1994**, *116*, 1595. (b) Corma, A.; Rey, F.; Thomas, J. M.; Sankar, G.; Greaves, G. N.; Cervilla, A.; Llopis, E.; Ribeira, A. *J. Chem. Soc., Chem. Commun.* **1996**, 1613. (c) Gago, S.; Pillinger, M.; Valente, A. A.; Santos, T. M.; Rocha, J.; Gonçalves, I. S. *Inorg. Chem.* **2004**, *43*, 5422. (d) Gago, S.; Dias, A. S.; Monteiro, B.; Pillinger, M.; Valente, A. A.; Santos, T. M.; Gonçalves, I. S. *J. Phys. Chem. Solids* **2006**, *67*, 1011.

(14) (a) Kühn, F. E.; Groarkei, M.; Bencze, É.; Herdtweck, E.; Prazeres, A.; Santos, A. M.; Calhorda, M. J.; Romão, C. C.; Gonçalves, I. S.; Lopes, A. D.; Pillinger, M. *Chem.—Eur. J.* **2002**, *8*, 2370. (b) Enemark, J. H.; Cooney, J. J. A.; Wang, J.-J.; Holm, R. H. *Chem. Rev.* **2004**, *104*, 1175.

(15) Arnaiz, F. J.; Aguado, R.; Sanz-Aparicio, J.; Martinez-Ripoll, M. *Polyhedron* **1994**, *13*, 2745.

Table 1. Conditions Used for the Preparation of the Intercalated LDHs

sample name[a]	solvent	precursor LDH/mg	precursor anion/mmol	total volume/mL
Zn−Al−Mo(50)	H_2O	430	1.08	40
Mg−Al−Mo(50)	H_2O	150	0.35	42
Li−Al−Mo(100)A	H_2O	250	2.88	15
Li−Al−Mo(100)B	H_2O	250	0.86	10
Li−Al−Mo(50)A	H_2O	250	1.73	15
Li−Al−Mo(50)B	H_2O	250	0.86	10
Li−Al−Mo(50)C[b]	H_2O/EtOH	100	1.15	26

[a] The reaction temperature (°C) is given in parentheses. [b] The ion exchange was repeated after the first 18 h treatment, using a fresh H_2O/EtOH (15/85 vol/vol) solution of complex **1**.

was maintained at 10 with a 2 M NaOH solution dosed using a Metrohm Model 718 Stat Titrino operating in the STAT mode. The resultant gel-like slurry was aged for 44 h at 70 °C, and the precipitate obtained was filtered, washed with DD water, and stored as an aqueous slurry in a closed container (total volume ~100 mL). For analysis, 20 mL of this slurry were filtered and the solid dried at room temperature under reduced pressure. Anal. Calcd for $[Mg_4Al_2(OH)_{12}](NO_3)_{1.74}(CO_3)_{0.13}\cdot 4.5H_2O$: Mg, 17.61; Al, 9.78; C, 0.28; H, 3.83; N, 4.41. Found: Mg, 17.5; Al, 9.8; C, 0.37; H, 3.57; N, 4.44%. TGA up to 250 °C revealed a sample weight loss of 11.3% (calcd for loss of $4.5H_2O$, 14.7%; for loss of $3H_2O$, 10.3%). IR (cm^{-1}): 3587sh, 3487br, 1635m, 1383vs, 826m, 670sh, 605s, 409s. Raman (cm^{-1}): 1053vs, 713w, 550m, 469w.

Li−Al−Cl LDH. The Li−Al layered precursor containing chloride anions with a Li/Al molar ratio of 0.5 was prepared by heating a suspension of gibbsite in an aqueous solution containing a 6-fold molar excess of lithium chloride in a Teflon-lined stainless steel autoclave for 2 days at 90 °C.[6e] Anal. Calcd for $[LiAl_2(OH)_6]Cl\cdot 2H_2O$: Li, 2.96; Al, 23.02; H, 4.3. Found: Li, 2.99; Al, 22.75; H, 3.98%. TGA up to 225 °C revealed a sample weight loss of 9.6% (calcd for loss of $2H_2O$, 15.3%; for loss of $1H_2O$, 8.3%). IR (cm^{-1}): 3550sh, 3451vs, 1625m, 944vs, 752s, 604s, 531vs, 457sh, 395sh, 377vs.

General Ion Exchange Procedure with Complex 1. The precursor LDH (solid Li−Al−Cl or a suspension of the Mg/Zn−Al LDHs in DD water) was added to a solution of **1** in DD water at room temperature, and the mixture was stirred with heating at either 50 or 100 °C for 18 h. The solid product was filtered, washed several times with DD water, and dried in vacuum at 50 °C. Table 1 gives the exact conditions used for each intercalation reaction. The intercalation of complex **1** into the Li−Al LDH was also carried out using a H_2O/EtOH (15/85 vol/vol) solvent mixture, giving a material designated as Li−Al−Mo(50)C.

Deintercalation of Li−Al−Mo(100)A. Li−Al−Mo(100)A (250 mg) was stirred in a D_2O solution (10 mL) of Na_2CO_3 (0.5 g, 4.7 mmol) overnight at room temperature. The mixture was filtered, and a portion of the dark yellow-brown filtrate reserved for analysis. ^1H NMR (300.13 MHz, Figure S10 in the Supporting Information): $\delta = 6.33$ (d, $J = 8.1$ Hz, dimer-H^5), 6.50 (d, $J = 8.7$ Hz, monomer-H^5), 6.83 (d, $J = 2.1$ Hz, dimer-H^2), 6.98 (dd, $J = 2.1$, 8.1 Hz, dimer-H^6), 7.12 (br, monomer-$H^{2,6}$). ICP-AES analyses of the solution and the residual solid indicated that 75% of the Mo atoms in the starting material were exchanged into solution.

Characterization Procedures. Microanalyses for CHN were carried out at the University of Aveiro. Li, Mg, Zn, Al, and Mo were determined by ICP-AES at the Central Laboratory for Analysis, University of Aveiro (by L. Carvalho). Conventional XRPD data were collected for all samples at room-temperature on an X'Pert MPD Philips diffractometer, equipped with an X'Celerator detector, a curved graphite monochromator (Cu Kα X-radiation, $\lambda = 1.54060$ Å), and a flat-plate sample holder, in a Bragg−Brentano para-focusing optics configuration (40 kV, 50 mA). Samples were step-scanned in 0.02° 2θ steps with a counting time of 1 s per step. The XRPD measurements as a function of temperature were carried out in situ using the same diffractometer equipped with an Anton-Parr GmbH HTK16 high temperature chamber containing a Pt heating filament and a Pt−Pt/Rh(10%) thermocouple. The powdered sample was deposited on the filament that also acts as sample holder. Heating rates of 10 °C min^{-1} were used. At a given temperature, samples were step-scanned in 0.05° 2θ steps with a counting time of 1 s per step. SEM with coupled EDS was carried out on a Hitachi SU-70 (S-4100) instrument using a 15 kV accelerating voltage. TGA and DSC were performed under air with Shimadzu TGA-50/DSC-50 systems at heating rates of 5 °C min^{-1}. IR spectra were obtained from KBr pellets using a FTIR Mattson-7000 spectrophotometer. Raman spectra were recorded on a Bruker RFS100/S FT instrument equipped with a InGaAs detector and using the 1064 nm excitation of the Nd:YAG laser. $^{13}C\{^1H\}$ CP/MAS NMR spectra were recorded at 125.72 MHz on a (11.7 T) Bruker Avance 500 spectrometer, with an optimized $\pi/2$ pulse for ^1H of 3.5 μs, 2 ms contact time, spinning rates of 7−10 kHz, and 4 s recycle delays. Chemical shifts are quoted in parts per million from tetramethylsilane. Diffuse reflectance UV−vis spectra were measured on a JASCO V-560 instrument using MgO as a reference.

X-ray Absorption Spectroscopy. Mo K-edge X-ray absorption spectra were measured at room temperature in transmission mode on Station 16.5 at the Daresbury Laboratory Synchrotron Radiation Source (DL SRS), operating at 2 GeV with currents between 150 and 230 mA. The order-sorting double Si(220) crystal monochromator was detuned to 70% of its maximum response to suppress harmonic contamination of the signal. Solid samples were diluted if necessary with BN and pressed into 13 mm pellets. Scans were set up to record the pre-edge at 10 eV steps and the postedge region in 0.04 $Å^{-1}$ steps, giving a total acquisition time of ~40 min per scan. In some cases, scans were summed to improve the data quality. The programs EXCALIB (DL SRS) and PYSPLINE[16] were used for calibration and background subtraction of the raw data. EXAFS curve-fitting analyses, by least-squares refinement of the non-Fourier filtered k^3-weighted EXAFS data, were carried out using the program EXCURVE (version EXCURV98[17]) using fast curved wave theory.[18] The calculations were performed using single scattering contributions. No improvements in the fits of the EXAFS of the intercalated LDHs were obtained by including multiple scattering contributions for the Mo−O−Mo bridging unit. Phase shifts were obtained within this program using ab initio calculations based on the Hedin Lundqvist/von Barth scheme. For each EXAFS simulation the validity of extra parameters was checked using a comparative reduced χ^2 method.[19]

Synchrotron X-ray powder Diffraction. High-resolution synchrotron XRPD data for Li−Al−Cl, Zn−Al−Mo(50), Li−Al−Mo(50)A, and Li−Al−Mo(100)A were collected at ambient temperature using the powder diffractometer at the ID31 beam line of the European Synchrotron Radiation Facility (ESRF), Grenoble, France.[20,21] The beam line receives X-rays from the synchrotron source, operating with an average energy of 6 GeV and a typical current of 200 mA

(16) Tenderholt, A.; Hedman, B.; Hodgson, K. O. *PySpline: A Modern, Cross-Platform Program for the Processing of Raw Averaged XAS Edge and EXAFS Data*; AIP Proceedings of the 13th International Conference on X-ray Absorption Fine Structure (XAFS13); American Institute of Physics: New York, 2007; Vol. *882*, 105−107.
(17) Binsted, N. *EXCURV98*, CCLRC Daresbury Laboratory computer programme; 1998.
(18) (a) Gurman, S. J.; Binsted, N.; Ross, I. *J. Phys. C* **1984**, *17*, 143. (b) Gurman, S. J.; Binsted, N.; Ross, I. *J. Phys. C* **1986**, *19*, 1845.
(19) O'Donnell, K. P.; Mosselmans, J. F. W.; Martin, R. W.; Pereira, S.; White, M. E. *J. Phys.: Condens. Matter* **2001**, *13*, 6977.

from an undulator device. The high signal-to-noise ratio of the data is because of the high brilliance of the synchrotron beam in combination with the use of a Si(111) crystal multianalyzer. The monochromatic wavelength employed was 0.93370(2) Å, which was calibrated against the Si standard NIST 640c [certified cell parameter $a = 5.4311946(92)$ Å].

Finely powdered samples were placed inside Hilgenberg borosilicate glass capillaries (diameter 0.7 mm) and rotated at 3 kHz during data collection to improve powder averaging over the individual crystallites, thus avoiding textural effects such as preferential orientation. Data were collected in a continuous-scanning mode ($\sim 10°\ 2\theta\ \text{min}^{-1}$ to eliminate the dead time of a conventional step scan) over the angular range $2-25°\ 2\theta$. The counts of eight detectors covering roughly $8°\ 2\theta$ were normalized to give the equivalent step scans. For each material a set of four data acquisitions were performed on the same volume of the sample. These consecutive data sets were not rebinned and normalized to produce a new pattern with higher signal-to-noise ratio because all materials exhibited mild radiation damage with increasing exposure times (as shown by a broadening of the peaks and a decrease in overall intensity), a known feature of high scintillation synchrotron sources. This effect was especially evident for the trace amount of the impurities appearing in the patterns of Li−Al−Mo(50)A and Li−Al−Mo(100)A. Since the angular regions for which these impurities appear have been omitted from the calculations, only broadening with increasing angle seems to affect the patterns used for the studies described in this work.

Collected XRPD patterns were indexed by means of the routines provided with the software program DICVOL04[22] and by employing the first 15 to 20 well-resolved reflections located using the derivative-based peak search algorithm provided with Fullprof.2k[23,24] and a fixed absolute error on each line of $0.03°\ 2\theta$. Unit cell metrics were obtained with high figures-of-merit. Analysis of the observed systematic absences were performed using the checkgroup subroutines provided with Fullprof Suite in parallel with the software package CHECKCELL,[25] leading to the unambiguous identification of the appropriate space groups for each material. Le Bail whole-powder-diffraction-pattern decompositions were computed using FullProf.2k with a fixed background determined by linear interpolation between consecutive (and manually selected) breakpoints in the powder patterns. Pseudo-Voigt or Pearson profile functions, along with one or two asymmetry correction parameters, were selected to generate the line shapes of the simulated diffraction peaks, and the angular dependence of the full-width-at-half-maximum (fwhm) of peaks was also taken into account by employing Caglioti corrections.[26] Typically, broadening of the individual reflections because of size effects was also considered by selecting a size model for plate-shaped crystallites with a defining [110] vector.[27] For all the materials, it was not possible to select an individual peak shape function which fully described the entire pattern. We attribute this to radiation damage of the samples which progressively broadens the peaks with increasing 2θ angle, ultimately resulting in the intensity and fwhm discrepancies observed for the simulated patterns. Nevertheless, integrated intensity data was used in conjunction with the GFourier software package[28] to reconstruct the electron density maps of the native Li−Al−Cl LDH and the intercalated Zn−Al−Mo(50), Li−Al−Mo(50)A, and Li−Al−Mo(100)A materials. A related strategy was described by Takagi and collaborators who calculated one-dimensional profiles along the interlayer spaces by only selecting the (00*l*) reflections.[29] A similar procedure aimed at the location of strong diffracting elements by Patterson synthesis has been adopted by Kanatzidis and collaborators.[30] The computational method we have employed in this study is significantly more robust because it accounts for the entire reflection data set extracted from the collected powder patterns and, therefore, allows the synthesis of three-dimensional maps (either Fourier or Patterson, not shown).

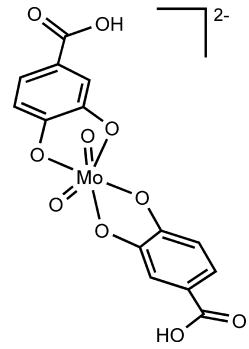

Figure 1. Complex **1**.

Full structure solutions employing integrated data for Li−Al−Cl and Li−Al−Mo(100)A were carried out using the direct methods of SIRPOW, included in the software package EXPO2004 (version 2.1).[31] After subtraction of the background using individual polynomial functions in selected angular intervals, the intensity of each individual reflection was extracted by employing Pearson profile functions. This strategy led to the ab initio unequivocal location of lithium and aluminum atoms, thus providing additional evidence for the structural integrity of the anionic layers in the intercalated material.

Le Bail whole-powder-diffraction-pattern decompositions along with refined profile and structural parameters for the Li−Al−Cl, Li−Al−Mo(50)A, and Li−Al−Mo(100)A LDHs are provided as Supporting Information.

Results and Discussion

Intercalation Study. Aqueous solutions of complex **1** (Figure 1) were mixed with the LDH precursors Zn−Al−NO_3 (Zn/Al = 1.9), Mg−Al−NO_3 (Mg/Al = 2.0), and

(20) Fitch, A. N. *J. Res. Natl. Inst. Stand. Technol.* **2004**, *109*, 133.
(21) Fitch, A. N. *The High Resolution Powder Diffraction Beam Line at ESRF in European Powder Diffraction: Epdic IV, Pts 1 and 2*; Transtec Publications Ltd, Zurich-Uetikon, 1996; *Vol. 228*, pp 219−221.
(22) Boultif, A.; Louer, D. *J. Appl. Crystallogr.* **2004**, *37*, 724.
(23) Roisnel, T.; Rodríguez-Carvajal, J. *Mater. Sci. Forum* **2001**, *378−381*, 118–123, WinPLOTR [February 2008], A Windows Tool for Powder Diffraction Pattern Analysis, Proceedings of the Seventh European Powder Diffraction Conference (EPDIC 7).
(24) Rodriguez-Carvajal, J. *FULLPROF: A Program for Rietveld Refinement and Pattern Matching Analysis*; Abstract of the Satellite Meeting on Powder Diffraction of the XV Congress of the IUCR, Toulouse, France; 1990, p. 127.
(25) Laugier, J.; Bochu, B. *CHECKCELL, A Software Performing Automatic Cell/Space Group Determination*; Collaborative Computational Project Number 14 (CCP14); Laboratoire des Matériaux et du Génie Physique de l'Ecole Supérieure de Physique de Grenoble (INPG): Grenoble, France, 2000.
(26) Caglioti, G.; Paoletti, A.; Ricci, F. P. *Nucl. Instr.* **1958**, *3*, 223.
(27) Snyder, R. L.; Fiala, J.; Bunge, H. J. *Defect and Microstructure Analysis by Diffraction*; IUCr Monographs on Crystallography; Oxford University Press, Cornwall, U.K., 2000; Vol. *10*.
(28) Gonzales-Platas, J.; Rodriguez-Carvajal, J. GFourier version 04.06 (March 2007).
(29) Itoh, T.; Shichi, T.; Yui, T.; Takahashi, H.; Inui, Y.; Takagi, K. *J. Phys. Chem. B* **2005**, *109*, 3199.
(30) Liu, Y.-J.; Schindler, J. L.; DeGroot, D. C.; Kannewurf, C. R.; Hirpo, W.; Kanatzidis, M. G. *Chem. Mater.* **1996**, *8*, 525.
(31) Altomare, A.; Burla, M. C.; Camalli, M.; Carrozzini, B.; Cascarano, G. L.; Guagliardi, A.; Giacovazzo, C.; Moliterni, A. G. G.; Polidori, G.; Rizzi, R. *J. Appl. Crystallogr.* **1999**, *32*, 339.

Table 2. Summary of the Elemental Analysis Data for the Intercalated LDHs

	chemical composition (wt %)[a]						atomic ratios[b]				
materialy, *z*, *n*[c]	Li, Mg, Zn	Al	Mo	C	H	N	Li, Mg, Zn	Al	Mo	C	C/Mo
Zn−Al−Mo(50) 0.33, 0.23, 5	25.68 (25.66)	6.58 (6.58)	10.44 (10.42)	11.45 (11.47)	2.38 (2.92)	0.34	3.22, *3.21*	2.00, *2.00*	0.89, *0.85*	7.82	8.8
Mg−Al−Mo(50) 0.05, 0.56, 13	10.80 (11.02)	6.25 (6.37)	7.23 (7.36)	12.24 (12.01)	3.47 (4.92)	0.25	3.84	2.00	0.65	8.80	13.5
Li−Al−Mo(100)A 0.17, 0.17, 5	1.58 (1.59)	12.70 (12.71)	11.60 (11.55)	13.52 (13.59)	4.25 (4.29)		0.97	2.00, *2.00*	0.51, *0.50*	4.78	9.4
Li−Al−Mo(100)B 0.10, 0.08, 3.5	1.75 (1.75)	17.00 (17.05)	8.39 (8.49)	9.48 (9.57)	4.11 (4.48)		0.80	2.00, *2.0*	0.28, *0.30*	2.51	9.0
Li−Al−Mo(50)A 0.16, 0.10, 5	1.57 (1.56)	14.10 (13.97)	10.40 (10.43)	11.37 (11.23)	4.08 (4.58)		0.87	2.00	0.42	3.62	8.6
Li−Al−Mo(50)B 0.12, 0.05, 3	2.03 (2.00)	18.00 (17.64)	9.30 (9.09)	9.39 (9.23)	3.96 (4.28)		0.88	2.00, *2.00*	0.29, *0.32*	2.34	8.1
Li−Al−Mo(50)C 0.03, 0.22, 7	1.36 (1.37)	13.50 (13.63)	6.46 (6.54)	10.24 (10.32)	3.99 (5.46)		0.78	2.00	0.27	3.41	12.6

[a] Determined by ICP-AES. [b] Values determined by SEM-EDS are given in italics. [c] Values used in the general formulas $[M'_xAl_2(OH)_{2(x+2)}]D_yM_z \cdot nH_2O$ (M′ = Mg, Zn) and $[Li_xAl_2(OH)_6]D_yM_z \cdot nH_2O$ to generate the calculated values given in parentheses, where $x/2$ is the M′/Al or Li/Al atomic ratio determined by ICP-AES, D (dimer) = $[Mo_2O_5(3,4\text{-dhb})_2]^{m-}$, M (monomer) = $[MoO_2(3,4\text{-dhb})_2]^{m-}$, and the ratio y/z was calculated from the bulk C/Mo atomic ratio.

Li−Al−Cl (Li/Al = 0.5) to give intercalated materials referred to as Zn−Al−Mo(*T*), Mg−Al−Mo(*T*), and Li−Al−Mo(*T*)A-C (Table 1). The chemical compositions of the products varied considerably according to the type of LDH precursor, the temperature of the exchange reaction (*T*), and the excess of complex **1** used (Table 2). For the two materials prepared from the Zn−Al−NO_3 and Mg−Al−NO_3 precursors, microanalysis for N showed that at least 90% of nitrate anions were exchanged. The C/Mo atomic ratio of 13.5 for Mg−Al−Mo(50) is close to the expected value of 14 for intercalated $[MoO_2(3,4\text{-dhb})_2]^{m-}$ anions. A lower ratio of 8.8 was found for Zn−Al−Mo(50), which is more consistent with a stoichiometry of one 3,4-dhb ligand per molybdenum. With the exception of the sample Li−Al−Mo(50)C, which was prepared using a H_2O/EtOH solvent mixture, low C/Mo atomic ratios in the range of 8.1−9.4 were also found for the Li−Al products. The Li/Al atomic ratios for these samples were in the range of 0.4−0.5, indicating that a certain fraction (no more than 20%) of Li in the starting LDH was leached into solution during some of the exchange reactions. For Li−Al−Mo(50)B and Li−Al−Mo(100)B, where the initial amounts of LDH precursor and complex **1** were the same, the increase in temperature did not lead to a higher molybdenum loading; in fact a slightly higher loading was obtained for the sample prepared at 50 °C. On the other hand, using a larger excess of complex **1** did lead to significantly higher Mo (and C) contents, with the highest value being 11.6 wt % for Li−Al−Mo(100)A.

SEM-EDS analysis was performed to complement the elemental analysis results for the Mo-containing samples, providing information about the concentrations of different elements in selected areas of the outermost regions of the LDH particles. Figure 2 displays SEM images of representative particles for the samples Li−Al−Cl and Li−Al−Mo(100)A. It is clear that the size, shape, and morphology of the particles are essentially the same, with both samples showing some fracturing of the crystals along the basal plane. Employing an elemental mapping technique, spatial elemental profiles were generated and are shown for the particles viewed "side-on." Profiles for a hexagonal Li−Al−Cl platelet viewed "face-on" are given in the Supporting Information. The

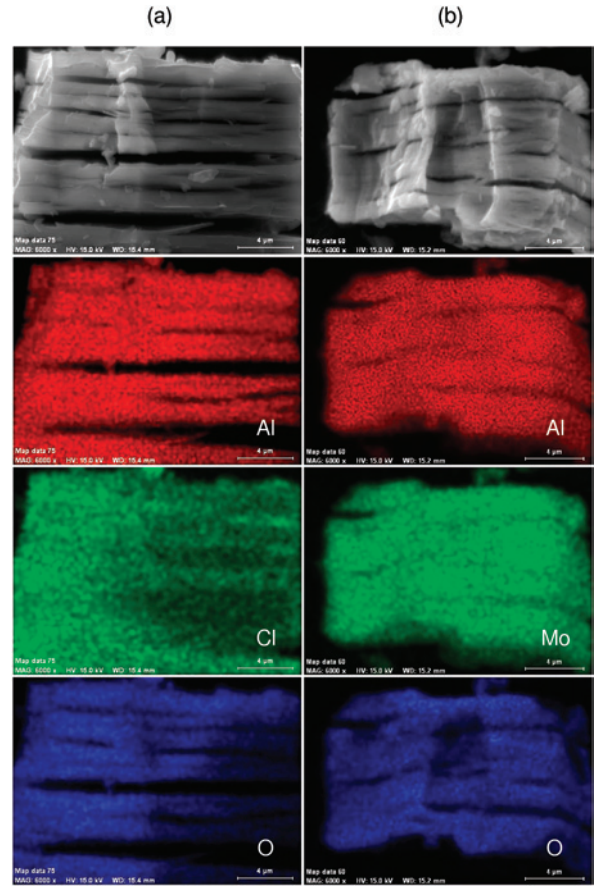

Figure 2. SEM images and corresponding elemental maps for (a) Li−Al−Cl and (b) Li−Al−Mo(100)A. The scale bar is 4 μm in all images.

profiles reveal a homogeneous distribution of either aluminum and chlorine atoms (for Li−Al−Cl) or aluminum and molybdenum atoms [for Li−Al−Mo(100)A] across the particles. EDS analysis of Li−Al−Mo(100)A on both the sides and faces of particles showed that the Mo/Al ratio was consistently in the range 0.24−0.26, which is in very good agreement with the bulk composition determined by ICP-AES (Table 2). Furthermore, no chlorine was detected, showing that the ion exchange had gone to completion. Minor quantities of chlorine (Al/Cl = 100−200) were detected for Li−Al−Mo(100)B and Li−Al−Mo(50)B. For

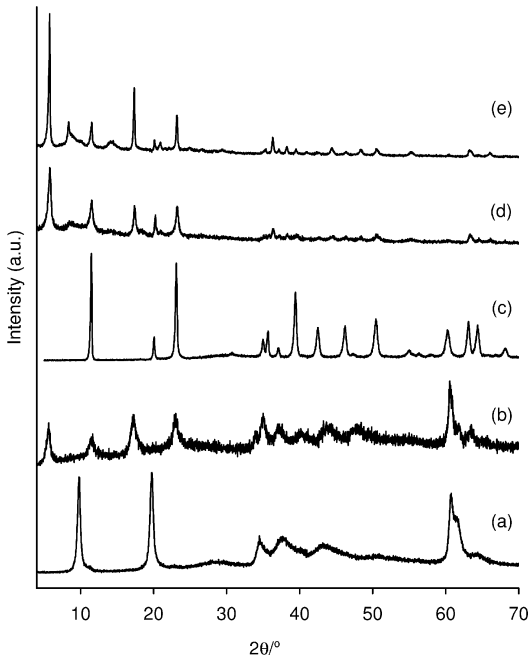

Figure 3. Conventional XRPD patterns of (a) Mg−Al−NO_3, (b) Mg−Al−Mo(50), (c) Li−Al−Cl, (d) Li−Al−Mo(100)B, and (e) Li−Al−Mo(100)A.

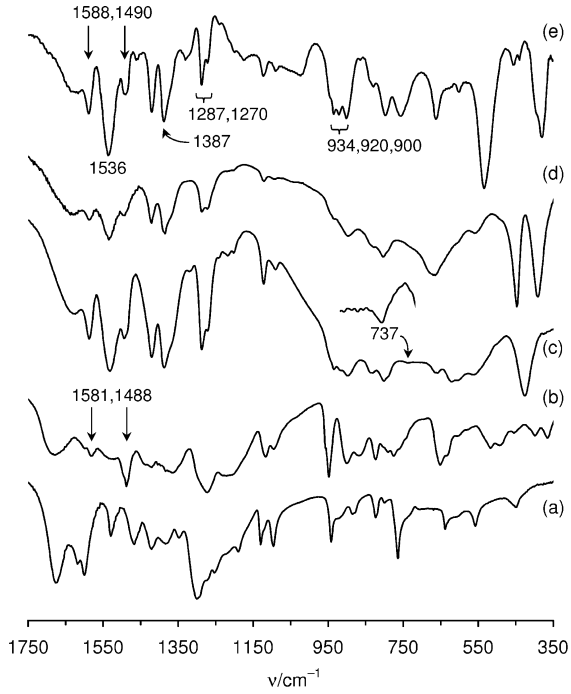

Figure 4. Infrared spectra (transmission mode) of (a) 3,4-dihydroxybenzoic acid, (b) complex **1**, (c) Zn−Al−Mo(50), (d) Mg−Al−Mo(50), and (e) Li−Al−Mo(100)A.

these two materials and Zn−Al−Mo(50), the average Mo/Al and Zn/Al ratios determined by EDS agreed, within experimental error, with the ICP-AES results. As found for Li−Al−Mo(100)A, the EDS mapping microimages for the elements Zn, Al, and Mo in Zn−Al−Mo(50) indicated a fairly even distribution across the surface of representative particles (Supporting Information).

Figure 3 shows the conventional laboratory-based XRPD patterns collected for the precursor LDHs and selected intercalated materials; the patterns for the remaining materials are given as Supporting Information. Synchrotron XRPD studies of Zn−Al−NO_3 on ID31 at the ESRF revealed the presence of a poorly crystalline material (data not shown). A trace amount of crystalline ZnO (zincite) was detected. Nevertheless, the considerably broad reflections arising from the Zn−Al−NO_3 layered material could be indexed and refined with a hexagonal unit cell [$a = b = 2 \times d_{110} =$ 3.067(1) Å; $c = 3 \times d_{003} = 26.625(2)$ Å] having rhombohedral symmetry ($R\bar{3}$m), in good agreement with the structures reported by Legrouri et al.[32] For Li−Al−Cl, the collected synchrotron XRPD pattern revealed the presence of a highly crystalline material which was unequivocally identified as being identical to the phase reported by Besserguenev et al.(see the Supporting Information for a Le Bail profile matching and reconstructed Fourier maps of the cationic layers and interstitial species).[3a]

The conventional XRPD patterns of all the intercalated LDHs prepared by ion exchange with complex **1** share a common feature, which is the appearance of four almost equally spaced Bragg reflections at low angles (5−25° 2θ). These peaks can be tentatively assigned as the (00l) reflections for an expanded phase with a basal spacing (given by the position of the first peak) of about 15.4 Å. This was confirmed by analysis of synchrotron XRPD patterns (described below after consideration of the spectroscopic characterization). The patterns for the Li−Al intercalated LDHs contain additional features of variable intensity in the 2θ ranges 7.5−10.5° and 13.5−15.5°, which are probably caused by a byproduct. The relative amount of this impurity phase seems to be very small since, even for Li−Al−Mo(100)A, where the additional reflections are more intense, there was no indication of a second phase in the SEM-EDS analyses. Furthermore, the XRPD patterns indicate that the appearance of this feature can be prevented by reducing the excess of complex **1** used, lowering the reaction temperature, or carrying out the exchange using a water/ethanol solvent mixture (at the expense of having a less crystalline 15 Å phase).

Spectroscopic Studies. To obtain information about the structure of the oxomolybdenum guest species in the intercalated LDHs, various spectroscopic studies were carried out. The vibrational spectra of the Mo-containing materials were all quite similar with respect to the bands arising from the guest species. In Figure 4 the IR spectra of Zn−Al−Mo(50), Mg−Al−Mo(50), and Li−Al−Mo(100)A are compared with those for 3,4-H_2dhb and complex **1**. The aromatic ring stretching bands at 1492 ± 2 (involving the C−C bond between the two oxygen atoms of the 3,4-dhb ligand[33,34]) and 1587 ± 1 cm^{-1} for the intercalated LDHs are essentially unshifted compared with the corresponding bands for **1**. The deprotonation of the carboxylic acid group is evidenced by

(32) Legrouri, A.; Badreddine, M.; Barroug, A.; De Roy, A.; Besse, J. P. *J. Mater. Sci. Lett.* **1999**, *18*, 1077.

(33) Lynch, M. W.; Valentine, M.; Hendrickson, D. N. *J. Am. Chem. Soc.* **1982**, *104*, 6982.

(34) Griffith, W. P.; Pumphrey, C. A.; Rainey, T.-A. *J. Chem. Soc., Dalton Trans.* **1986**, 1125.

Table 3. Mo K-Edge EXAFS-Derived Structural Parameters

compound	atom	CN[a]	r/Å	$2\sigma^2$/Å^2[b]	E_f/eV[c]	R/%[d]
$[MoO_2Cl_2(DMF)_2]$	O	1.8(1)	1.705(1)	0.0033(1)	4.8(4)	13.3
	O	2.0(2)	2.322(9)	0.0085(3)		
	Cl	2.0(2)	2.375(3)	0.0250(49)		
1	O	1.4(1)	1.730(1)	0.0020(1)	3.0(4)	13.3
	O	1.0(2)	2.005(3)	0.0045(5)		
	O	1.0(2)	2.148(6)	0.0103(14)		
	C	2.0(4)	2.975(9)	0.0101(17)		
Zn−Al−Mo(50)	O	1.6(1)	1.723(2)	0.0019(2)	5.8(6)	21.9
	O	0.9(2)	1.964(5)	0.0055(11)		
	Mo	0.6(1)	3.168(4)	0.0056(5)		
Mg−Al−Mo(50)	O	1.6(1)	1.728(1)	0.0025(1)	7.4(4)	13.4
	O	0.6(1)	1.983(4)	0.0049(8)		
	Mo	0.35(1)	3.164(3)	0.0047(4)		
Li−Al−Mo(100)A	O	1.6(1)	1.720(2)	0.0025(2)	6.1(5)	18.6
	O	1.0(1)	1.965(3)	0.0039(6)		
	Mo	0.6(1)	3.163(3)	0.0049(4)		
Li−Al−Mo(50)A	O	1.6(1)	1.723(1)	0.0024(1)	5.0(4)	14.4
	O	1.0(1)	1.964(3)	0.0043(4)		
	Mo	0.6(1)	3.162(2)	0.0049(3)		
Li−Al−Mo(50)B	O	1.6(1)	1.723(1)	0.0024(2)	6.1(5)	19.5
	O	1.0(1)	1.965(3)	0.0046(6)		
	Mo	0.6(1)	3.161(3)	0.0048(3)		

[a] CN = Coordination number. Values in parentheses are statistical errors generated in EXCURVE. The true errors in coordination numbers are likely to be on the order of 20%; those for the interatomic distances are ~1.5%.[35] [b] Debye−Waller factor; σ = root-mean-square internuclear separation. [c] E_f = edge position (Fermi energy), relative to calculated vacuum zero. [d] $R = (\int[\Sigma^{theory} - \Sigma^{exptl}]k^3dk/[\Sigma^{exptl}]k^3dk) \times 100\%$.

the absence of a ν_{asym}(C═O) vibration at ~1680 cm^{-1} and the appearance of two strong bands attributable to $\nu_{sym}(CO_2)$ (1387 ± 2 cm^{-1}) and $\nu_{asym}(CO_2)$ (1534 ± 2 cm^{-1}) vibrations. As found for complex **1**, all of the intercalated LDHs exhibit a band at about 1270 cm^{-1} for the ν(C−O) ligand vibration, which is characteristic of catecholate coordination.[33,34] These observations were previously taken as evidence for the intercalation of structurally intact $[MoO_2(3,4\text{-dhb})_2]^{m-}$ anions in the material Zn−Al−Mo(50).[13d] However, the 1270 cm^{-1} band appears as a shoulder on a second, generally more intense band at 1287 cm^{-1}, which can also be assigned to the stretching of deprotonated, metal-coordinated C−O groups. The presence of this band indicates a modification of the coordination mode for at least some of the 3,4-dhb ligands.

In complex **1**, the symmetric Mo═O stretching vibration for the *cis*-MoO_2^{2+} unit appears at 900 cm^{-1} as a strong band in the Raman, weaker in the IR, with the asymmetric stretch medium in the IR and weaker in the Raman, at about 868 cm^{-1}. A strong band at 947 cm^{-1} is associated with the organic ligand. While a band is present at 895−900 cm^{-1} in the IR (and 892 cm^{-1} in the Raman) for the intercalated LDHs, no band is observed around 868 cm^{-1} (Figure 4). Furthermore, the Mo-containing Zn−Al and Li−Al materials show additional IR bands at 920 and 934 cm^{-1} and a medium intensity Raman band at 930 cm^{-1}, all of which can be assigned to Mo═O stretching vibrations. The IR spectrum of Mg−Al−Mo(50) is slightly different in that only the 934 cm^{-1} band is observed as a shoulder on the more intense absorption at 895 cm^{-1}. Below 850 cm^{-1}, the vibrational spectra of the intercalated LDHs contain some bands caused by the guest species in addition to bands arising from MO vibrations and MOH bending of the LDH host structures. As indicated in Figure 4, the material Zn−Al−Mo(50) exhibits a weak absorption at 737 cm^{-1} that is not exhibited by the LDH−nitrate precursor or complex **1**. Taking into account the EXAFS results described below, we may tentatively assign this band to the asymmetric stretching vibration, $\nu_{asym}(Mo_2O)$, of oxomolybdenum(VI) complexes containing bridging μ-oxo groups (Mo−O−Mo).[34]

Mo K-edge EXAFS studies were carried out to get a more conclusive picture of the average structural environment of the molybdenum centers in the intercalated LDHs. Analysis of the raw k^3-weighted EXAFS data for the model compound $[MoO_2Cl_2(DMF)_2]$ gave a first coordination sphere of 1.8 oxygen atoms at 1.70 Å, 2.0 oxygen atoms at 2.32 Å, and 2.0 chlorine atoms at 2.37 Å (Table 3; the EXAFS spectra and Fourier transforms (FTs) are given in the Supporting Information), which is consistent with the expected distorted octahedral coordination geometry consisting of a *cis*-MoO_2 unit, two chlorine atoms and two DMF oxygen atoms. The refined Mo═O and Mo−Cl distances are in reasonable agreement with the crystallographic values of 1.68 and 2.34 Å,[36] while the Mo−O_{DMF} distance is significantly longer than the reported value of 2.20 Å. The EXAFS-derived distance may be unreliable because of high correlations between the parameters for this shell and those for the chlorine shell. For $(NMe_4)_2[MoO_2(3,4\text{-dhb})_2]\cdot 2H_2O$ (**1**), the initial model consisted of three oxygen shells at 1.73, 2.01, and 2.15 Å, with coordination numbers of 1.4, 1.0, and 1.0. The first shell can be assigned to terminal oxo ligands and the other two shells to deprotonated 3,4-oxygen atoms of the organic ligand. The presence of the organic ligand was confirmed by addition of a fourth shell for carbon atoms at 2.98 Å, which improved the goodness-of-fit R-factor from 17.5 to 13.3% (Figure 5, Table 3). A single-crystal X-ray diffraction study of the tetramethylammonium salt has shown that the molybdenum atom in the anion $[MoO_2(3,4\text{-dhb})_2]^{2-}$ has a distorted octahedral coordination geometry consisting of a

(35) Evans, J.; Gauntlett, J. T.; Mosselmans, J. F. W. *Faraday Discuss., Chem. Soc.* **1990**, 107.
(36) Florian, L. R.; Corey, E. R. *Inorg. Chem.* **1968**, *7*, 722.

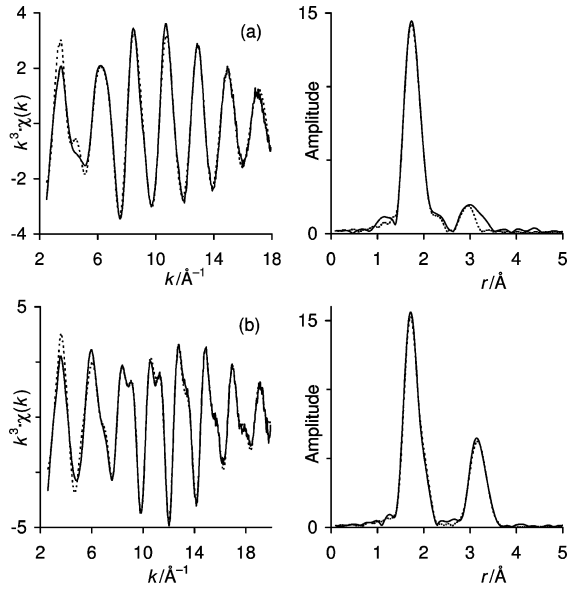

Figure 5. Mo K-edge k^3-weighted EXAFS and Fourier transforms of (a) $(NMe_4)_2[MoO_2(3,4\text{-dhb})_2]\cdot 2H_2O$ (**1**) (sum of two scans) and (b) Li−Al−Mo(50)A. The solid lines represent the experimental data and the dashed lines show the fits obtained using the parameters given in Table 3.

cis-MoO_2 unit (Mo═O 1.705, 1.721 Å) and four catecholate oxygen atoms (Mo−O_{cat} 1.977, 2.007, 2.128, 2.138 Å).[37] Although the EXAFS-derived distances are in acceptable agreement with the crystallographic data, the refined coordination numbers are lower than expected, especially concerning the two Mo−O_{cat} shells. These values should be treated with some caution because the refinement of coordination numbers and Debye−Waller factors simultaneously does not always give reliable results because of the high correlation of the two parameters. In addition, the total number of oxygen neighbors in a given shell may be underestimated if there is a high degree of anharmonic static disorder (multiple Mo···O interatomic distances).

Figure 5 shows the raw k^3-weighted EXAFS data for the material Li−Al−Mo(50)A. The spectra for the other materials are provided as Supporting Information. Solely on the basis of the raw data, the intercalated LDH spectra show a strong similarity, but are clearly different from that for complex **1** in terms of the phase and amplitude of all the features in k space. The r-space plots of the Fourier-transformed EXAFS data for the intercalated LDHs show the presence of a strong interaction around 3 Å, which is not present in the FT for **1**. All of the spectra for the intercalated LDHs could be satisfactorily modeled using oxygen shells at 1.72−1.73 Å and 1.96−1.98 Å, and a molybdenum shell at 3.16−3.17 Å (Table 3). The addition of the third shell greatly improved the overall fit, for example the R-factor decreased from 40% to 18.6% for Li−Al−Mo(100)A. A further improvement in the fits was obtained through the addition of a fourth shell for oxygen atoms at 2.22−2.24 Å for the Li−Al and Zn−Al LDHs and 2.16 Å for the Mg−Al LDH. For example, in the case of Li−Al−Mo(50)A, the inclusion of this shell with a coordination number of 1.0 resulted in a decrease in the R-factor

(37) Manuscript in preparation.

Figure 6. Summary of the crystallographically determined interatomic distances in complexes containing the dianion $[Mo_2O_5L_2]^{2-}$ [L = 3,5-R_2catecholate (R = H, *t*Bu) and naphthalene-2,3-diolate].[39]

from 14.4 to 12.1% and a decrease in the reduced χ^2 value from 3.6×10^{-7} to 2.8×10^{-7}. However, the shell was not included in the final fits because of large statistical errors in the refined structural parameters, high Debye−Waller factors of 0.03−0.05 Å^2, and a reduced coordination number of 1.0, which imply a high degree of disorder.

The EXAFS-derived Mo···Mo interaction for the intercalated LDHs indicates the presence of dimers and/or higher oligomers, and the second oxygen shell at ca. 1.97 Å presumably has a contribution from oxygens which form a bridge between neighboring metal atoms. A search in the Cambridge Crystallographic Database (version 5.28, update Aug 2007)[38] revealed that a Mo···Mo separation around 3.15 Å is very typical of bis(catecholate) complexes of the type $[Mo_2O_5L_2]^{2-}$ containing cofacially oriented catecholate subunits (L) bridged by a $[(MoO_2)_2(\mu\text{-O})]^{2+}$ core. Figure 6 summarizes the interatomic distances determined from crystallographic data for complexes with L = 3,5-R_2catecholate (R = H, *t*Bu) and naphthalene-2,3-diolate.[39] The data show that the first coordination sphere around each molybdenum atom is composed of four oxygen shells around 1.7, 1.95, 2.15 and 2.4 Å. Comparing the distances for the first two Mo−O shells and the Mo···Mo interaction with those determined by EXAFS for the intercalated LDHs, we may propose that a similar type of species is present in the intercalated LDHs. Indeed, the complex $[Mo_2O_5(H_2O)_2(3,4\text{-dhb})_2]^{2-}$ has been described by Karaliota et al. (as the tetraphenylphosphonium salt), although not structurally characterized.[40] There is a good match between the vibrational spectroscopic data reported for this complex [$\nu_{sym}(MoO_2)$ = 923 (IR) and 928 (Raman) cm^{-1}, $\nu_{asym}(MoO_2)$ = 892 cm^{-1} (IR), and ν(C−O)$_{cat}$ = 1286 cm^{-1} (IR)] and the bands exhibited by the Mo-containing Zn−Al and Li−Al LDHs.

The elemental analysis data for the materials Zn−Al−Mo(50), Li−Al−Mo(100)A, and Li−Al−Mo(50)A are also consistent with the intercalation of binuclear 1:1 (molybdenum:catecholate) species. Thus, assuming that the positive charges of the host layers are balanced exclusively by intercalated oxomolybdenum complexes, the average negative charge per Mo atom is given by the bulk Al/Mo [for

(38) (a) Allen, F. H. *Acta Crystallogr., Sect. B: Struct. Sci* **2002**, *58*, 380. (b) Allen, F. H.; Motherwell, W. D. S. *Acta Crystallogr., Sect. B: Struct. Sci.* **2002**, *58*, 407.
(39) (a) Tkachev, V. V.; Atovmyan, L. O. *Koord Khim* **1976**, *2*, 110. (b) Pierpont, C. G.; Buchanan, R. M. *Inorg. Chem.* **1982**, *21*, 652. (c) El-Hendawy, A. M.; Griffith, W. P.; O'Mahoney, C. A.; Williams, D. J. *Polyhedron* **1989**, *8*, 519. (d) Lu, X.-M.; Zhou, Y.-Z.; Liu, S.-C.; Mao, X.; Bu, X.-H. *Chem. Res. Chin. Univ.* **2002**, *18*, 228.
(40) Karaliota, A.; Kamariotaki, M.; Hadjipanagioti, D.; Aletras, V. *J. Inorg. Biochem.* **1998**, *69*, 79.

Zn−Al−Mo(50)] and Li/Mo atomic ratios. Values in the range of 1.9−2.2 were found for these three materials, which would be consistent with the presence of species like $[Mo_2O_5(3,4\text{-dhb})_2]^{4-}$ (rather than, or in addition to, $[MoO_2(3,4\text{-dhb})_2]^{4-}$) where the extra 2− charge comes from the deprotonation of the carboxylic acid groups. The bulk C/Mo atomic ratios tend to support this conclusion (Table 2), although the values never reach the expected value of 7 for the 1:1 complex. Given that the EXAFS-derived coordination number for the Mo···Mo shell is less than unity for the Zn−Al and Li−Al materials studied, the cointercalation of the mononuclear 1:2 species must be considered. Indeed, the observation of at least three IR-active $\nu(MoO_2)$ vibrations suggests the presence of more than one type of oxomolybdenum complex. For the material Mg−Al−Mo(50), the elemental analysis (C/Mo = 13.5) and EXAFS (CN = 0.35 for the Mo···Mo shell) data indicate that the distribution of different Mo species (monomer, dimer) is weighted toward having more of the monomer. This is also evident for the Li−Al material prepared using a H_2O/EtOH solvent mixture (C/Mo = 12.6). In Table 2, calculated compositional data are given for chemical formulas that assume that the charge-balancing guest species in the intercalated LDHs are the mononuclear 1:2 or binuclear 1:1 species. The bulk C/Mo molar ratios for the Zn−Al and Li−Al materials prepared using only water as solvent lead to a dimer/monomer molar ratio between 1 and 2.4, i.e. at least two-thirds of the Mo atoms are present as the dimer. Molar ratios of 0.09 and 0.14 were estimated for Mg−Al−Mo(50) and Li−Al−Mo(50)C. Apart from Li−Al−Mo(100)B and Li−Al−Mo(50)B, which were prepared using a smaller excess of complex **1** compared with the other Li−Al LDHs, the maximum theoretical charge supplied by the anionic guests in each chemical formula (obtained by multiplying the sum of y and z by four) is between 10 and 40% higher than the calculated positive charge of the host layers. This could be compensated for by partial protonation of the 3,4-dhb carboxylate groups. On the basis of the dimer/monomer molar ratios for the Zn−Al and Li−Al materials prepared using only water as solvent, the EXAFS-derived coordination number for the Mo···Mo shell should be 0.75 ± 0.1, which is in reasonable agreement with the actual value of 0.6 (allowing for an error of at least 20% in the latter value).

Complex **1** and its freshly prepared aqueous solution are deep red, which is the typical color of $[MoO_2(catecholate)_2]^{2-}$ complexes.[40−42] The yellow-brown color of the Zn−Al and Li−Al materials prepared using only water as solvent is another indication for the binuclear 1:1 complex being the major species intercalated because $[Mo_2O_5(catecholate)_2]^{2-}$complexes are usually yellow or pale orange. This was further investigated for the sample Li−Al−Mo(100)A by carrying out diffuse reflectance UV−vis spectroscopy (Supporting Information). The complex $(NMe_4)_2[MoO_2(3,4\text{-dhb})_2]\cdot 2H_2O$ (**1**) exhibits a very broad, intense absorption with a maximum around 475 nm. This is considered to be a catecholate-to-metal charge transfer transition. The spectrum of Li−Al−Mo(100)A is dominated by an absorption peak at ∼400 nm and a second weaker absorption, which appears as a shoulder around 475 nm. By comparison with the spectrum for **1**, the lower energy absorption can be attributed to a charge transfer transition of intercalated mononuclear 1:2 species. The charge transfer absorption band for $[Mo_2O_5(catecholate)_2]^{2-}$ dimers is generally shifted to lower wavelengths compared with that of the corresponding monomer, $[MoO_2(catecholate)_2]^{2-}$,[41] and hence the band at ∼400 nm is assigned to intercalated binuclear 1:1 species.

In an effort to obtain an alternative quantitative assessment of the different guest species present in the sample Li−Al−Mo(100)A, an experiment was performed to deintercalate the sample by anion exchange with carbonate anions and measure the ^{1}H NMR spectrum of the resultant solution (please see the Experimental Section for more details; the spectrum is provided in the Supporting Information). ICP-AES analyses of the solution and the residual solid indicated that 75% of the Mo atoms were exchanged into solution. The ^{1}H NMR spectrum contained several reasonably well-defined signals in the region of the aromatic ligand protons, which were assigned to $[Mo_2O_5(3,4\text{-dhb})_2]^{m-}$ (dimer) and $[MoO_2(3,4\text{-dhb})_2]^{m-}$ (monomer) species by comparison with literature data for similar complexes.[13d,34,40,41d,42,43] The ratio of the integrals for the two H^5 signals was approximately 1:1.1 (mononuclear:binuclear), which is in very good agreement with the monomer/dimer molar ratio estimated from the elemental analysis data (Table 2). Still, the ^{1}H NMR result must be treated with caution because the exchange was not complete, and one of the two guest species may be preferentially exchanged. Furthermore, upon dissolution, an equilibrium will likely exist between the different species that will be affected by the solution pH, the changing concentrations, and the presence of sodium/carbonate ions in solution.

Figure 7 shows the ^{13}C{^{1}H} CP/MAS NMR spectra of 3,4-H_2dhb, complex **1** and Li−Al−Mo(100)A. The signals at 142.4 and 150.6 ppm for the free ligand 3,4-H_2dhb are assigned to C^3 and C^4,[42] and the overlapping peaks between 114 and 126 ppm are the result of the remaining aromatic ring carbon atoms. The carboxylic acid group gives rise to a single resonance at 173.4 ppm. For complex **1**, catecholate bonding is indicated by the downfield shift of the resonances for C^3 and C^4 to 156.7 and 162.2 ppm.[42] Two broad signals at 113.5 and 123.9 ppm are observed for the remaining aromatic ring carbon atoms. The spectrum of Li−Al−Mo(100)A is representative of all the spectra recorded for the Mo-containing LDHs. Compared with complex **1**, the resonance for the carboxylate carbon atom is shifted downfield by about 4 ppm (from 170.2 to 174.5 ppm), and only one signal is observed for C^3 and C^4 at 156.1 ppm. These

(41) (a) Haight, G. P., Jr.; Paragamian, V. *Anal. Chem.* **1960**, *32*, 642. (b) Kustin, K.; Liu, S.-T. *J. Am. Chem. Soc.* **1973**, *95*, 2487. (c) Natansohn, S.; Krugler, J. I.; Lester, J. E.; Chagnon, M. S.; Flnocchlaro, R. S. *J. Phys. Chem.* **1980**, *84*, 2972. (d) Wilshire, J. P.; Leon, L.; Bosserman, P.; Sawyer, D. T. *J. Am. Chem. Soc.* **1979**, *101*, 3379.

(42) Griffith, W. P.; Nogueira, H. I. S.; Parkin, B. C.; Sheppard, R. N.; White, A. J. P.; Williams, D. J. *J. Chem. Soc., Dalton Trans.* **1995**, 1775.

(43) Litos, C.; Aletras, V.; Hatzipanayioti, D.; Kamariotaki, M.; Lymberopoulou-Karaliota, A. *Inorg. Chim. Acta* **2007**, *360*, 2321.

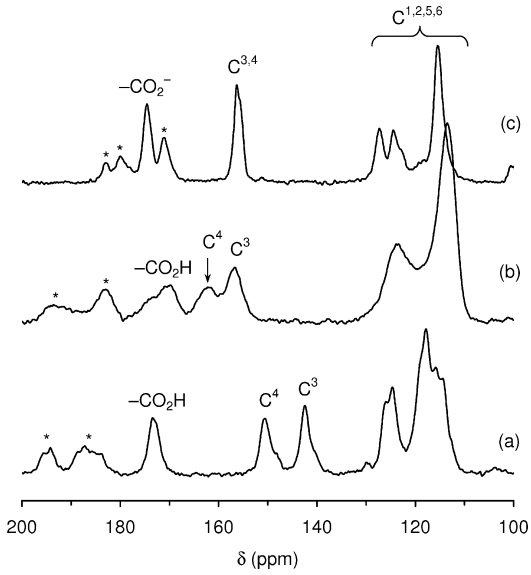

Figure 7. $^{13}C\{^1H\}$ CP/MAS NMR spectra of (a) 3,4-dihydroxybenzoic acid, (b) complex **1**, and (c) Li−Al−Mo(100)A. Spinning sidebands are indicated by an asterisk.

differences are attributed to deprotonation of the carboxylic acid group. Previous ^{13}C NMR studies of compounds containing the anions $[MoO_2(cat)_2]^{2-}$ and $[Mo_2O_5(cat)_2]^{2-}$ showed that the resonances of the carbon atoms bonded to the oxygens appear in the range 157−159 ppm (cf., 147 ppm for free catechol).[34] Therefore, although the spectra of the intercalated LDHs are clearly consistent with coordination of the phenolic oxygen atoms to Mo^{VI} centers (and no free ligand), they do not allow us to distinguish between the different types of catecholate bonding expected for the mononuclear and binuclear species.

Synchrotron XRPD Studies of the Intercalated LDHs. The high-resolution synchrotron XRPD patterns of Li−Al−Mo(50)A and Li−Al−Mo(100)A (Figures S11 and S12 in the Supporting Information) were unequivocally indexed with an expanded hexagonal unit cell (space group $P6_3/m$) for which, as in the original Li−Al−Cl material, the length of the *c*-axis (∼30.7 Å) encompasses two interlayer voids. Fourier maps (F_{obs}) calculated from the integrated intensities extracted from Le Bail profile decompositions show that: (1) the mixed Li−Al hydroxide layers retain their structural integrity and two-dimensional ordering after intercalation; (2) within each layer, the structural disorder between lithium and aluminum sites is minimal as clearly observed by the very distinct summed intensities represented in Figure 8a; (3) statistically disordered electron density is located in the interlayer spaces and periodically distributed; (4) the highest intensities for the interlayer electron density are found close to the Li−Al hydroxide layers [Figures 8b and S11b]. These results are fully compatible with a structural model based on the intercalation of dimeric bis(catecholate) complexes of the type described above. In this model the $[Mo_2O_5(3,4\text{-dhb})_2]^{4-}$ anions are positioned in such a way that the Mo → Mo vector is parallel to the Li−Al hydroxide layers and the overall orientation of the complex is perpendicular to the same layers, even though it could be disordered over, at least, two distinct positions as depicted in Figures 8b and S11b. From crystallographic studies of compounds containing the anions $[MoO_2(3,4\text{-dhb})_2]^{2-}$ and $[Mo_2O_5(cat)_2]^{2-}$,[37,39] we can estimate that the distance occupied by the anion in this orientation is ∼10.8 Å perpendicular to the layers, which fits well with the observed gallery height of 10.7 Å. Furthermore, this overall orientation maximizes the number and geometrical features of the possible O−H···O hydrogen bonding interactions (in which the carboxylate groups and Mo=O groups interact directly with the hydroxyl groups of the layers).

The material Zn−Al−Mo(50) also has an expanded structure as clearly observed by the *d*-spacing of the first reflection. However, the (00*l*) reflections envelope of the collected powder pattern could not be matched with analogous patterns for other materials, thus suggesting a longer *c*-axis for the compound in study. Indeed, the pattern could be unequivocally indexed with a hexagonal unit cell with a *c*-axis of 45.932(2) Å. Analysis of the systematic absences revealed that the overall symmetry of this intercalated material is better described in the $P6_4$ space group (Figure 9). Fourier maps (F_{obs}) calculated for Zn−Al−Mo(50) led to the same geometrical conclusions for the intercalation mode of dimeric species as those described above for the two Li−Al compounds, with the average gallery height being ∼10.6 Å. For this particular cationic layer the disorder between zinc and aluminum sites is structurally more significant and noticeable in the calculated Fourier maps. Figure 9a shows the integrated electron density along the *c*-direction for the region of the unit cell corresponding to these cationic layers and, from the density distribution, it is not possible to unequivocally assign the location of Al, Zn, and O.

The data extracted from the collected powder patterns clearly support the assumption of high disorder concerning the rotation of the guest species along the *c*-axis of the unit cell for all materials. If the anionic complexes were located at specific crystallographic positions within the unit cell, the higher *l*-ordered reflections, mainly located in the 14−21° 2θ range, should be observed with considerable intensity. For example, in the two intercalated materials Li−Al−Mo(50)A and Li−Al−Mo(100)A, this angular region does not contain any relevant reflections and it was excluded from the profile decompositions to achieve a better profile matching (see the Supporting Information).

Thermal Behavior. The thermal decomposition behaviors of Mg−Al−NO_3 and Mg−Al−Mo(50) were examined by TGA and DSC (Figure 10). The removal of physically adsorbed and structural (interlayer) water from Mg−Al−NO_3 takes place smoothly from room temperature to 180 °C, with a total weight loss of 11.3% at 250 °C. A corresponding broad endothermic signal peaking at 133 °C is observed in the DSC curve. For Mg−Al−Mo(50), a higher weight loss of 19.2% occurs up to 250 °C, and the TG and DSC curves

(44) Boultif, A.; Louer, D. *J. Appl. Crystallogr.* **1991**, *24*, 987.
(45) Louer, D. In *Automatic Indexing: Procedures and Applications, Accuracy in Powder Diffraction II*; Prince, E., Stalick, J. K., Eds.; National Institute of Standards and Technology, U.S. Department of Commerce: Gaithersburg, MD, 1992; pp. 92−104.

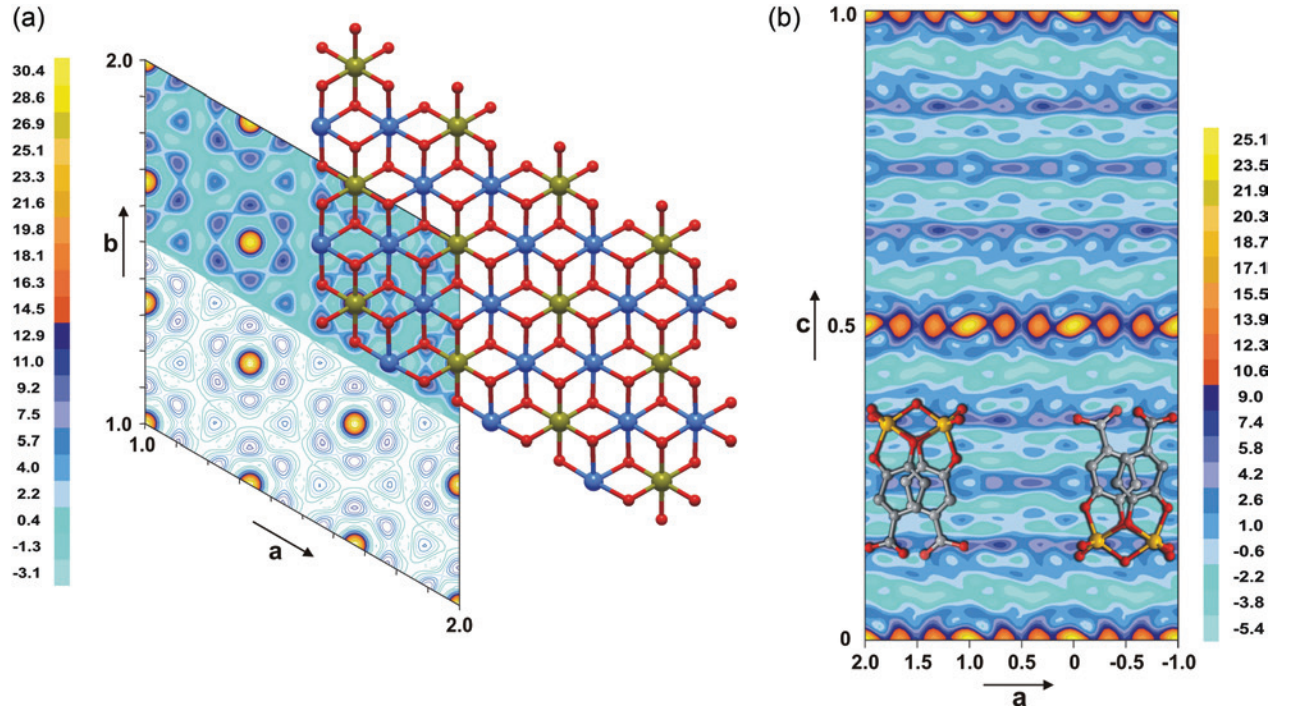

Figure 8. Fourier maps calculated by GFourier and by employing the F_{obs} extracted from a Le Bail whole-powder-diffraction-pattern decomposition of Li−Al−Mo(100)A [unit cell metrics: $a = b = 5.0915(1)$ Å, $c = 30.650(1)$ Å], summed from (a) −0.1 to 0.1 along the *c*-axis and from (b) 0 to 1 along the *b*-axis. The structural drawing of the cationic Li−Al layer solved from the powder pattern of Li−Al−Cl (Figure S3 in the Supporting Information) is overlaid in the image on the left, demonstrating that the cationic layers retain their structural integrity upon inclusion of the oxomolybdenum species (image on the right).

indicate that the sample loses interlayer water more easily. These differences may arise from having a more open structure with more easily accessible interlayer voids. The discrepancy between the 19.2% weight loss and the value of 27.6% calculated for the chemical formula given in Table 2 (with 13 water molecules) may be the result of the presence of strongly held water molecules that are only removed at temperatures close to 300 °C. For Mg−Al−NO_3, a mass loss of 35.4% takes place in the range 280−600 °C, attributed to the dehydroxylation of the brucite-like layer and the loss of interlayer nitrate anions. These overlapping processes give rise to a broad and intense endothermic peak in the DSC curve in the range 280−460 °C, with a peak temperature of 405 °C. In the DSC curve for Mg−Al−Mo(50) an exothermic peak centered at 320 °C precedes the endothermic dehydroxylation step at 390 °C, and a weight loss of 34.5% takes place between 200 and 600 °C. By comparison with the DSC plot for complex **1** (not shown), the feature at ∼320 °C can be assigned to the oxidative degradation of the organic ligands associated with the intercalated complexes (cf., a peak temperature of 310 °C for complex **1**).

The thermal behavior of Mg−Al−Mo(50) was further studied by measuring XRPD diagrams at increasing temperatures (Figure 11). Heating the sample to 50 °C did not induce significant changes apart from a slight decrease in the intensities of the 00*l* reflections. At 75 °C, the basal reflection at ∼15.5 Å is much weaker and overlaps with a new peak at about 13 Å that is indicated by an asterisk in Figure 11. This new peak persists up to 370 °C, undergoing a gradual shift toward higher angles, while the 00*l* peaks corresponding to the initial Mg−Al−Mo(50) phase are only discernible up to about 160 °C and do not shift noticeably with increase in temperature. We may tentatively assign the new peak to a collapsed phase that forms as a result of a reorientation of the intercalated oxomolybdenum complexes between 50 and 100 °C, presumably because of removal of interlayer water molecules. Between 100 and 300 °C, a second very broad peak can be seen around 20° 2θ, which seems to be associated with the new phase because it also undergoes a shift toward higher angles with increase in temperature. The samples heated to 450 and 600 °C are essentially amorphous. In our previous report, we described the thermal behavior of a Zn−Al−Mo(50) intercalate with Zn/Al = 2, prepared by treatment of a Zn−Al−NO_3 precursor with an aqueous solution of complex **1**.[13d] Upon heating the Zn−Al sample no collapsed phase formed, and the 15 Å phase was present up to 160 °C. The different behaviors exhibited by the Mg−Al and Zn−Al samples are presumably related with having mostly mononuclear 1:2 species intercalated in the Mg−Al sample, and binuclear 1:1 species in the Zn−Al sample.

The thermal stability of the Li−Al materials was also investigated by TGA (Supporting Information). The TG curve of the starting material, Li−Al−Cl, was in agreement with that reported previously,[46] showing the loss of surface water from room temperature up to about 65 °C, followed by the removal of interlayer water up to 150 °C, and dehydroxylation and partial dechlorination around 340 °C. All the Mo-containing samples presented nearly identical

(46) Hou, X.; Kirkpatrick, R. J. *Inorg. Chem.* **2001**, *40*, 6397.

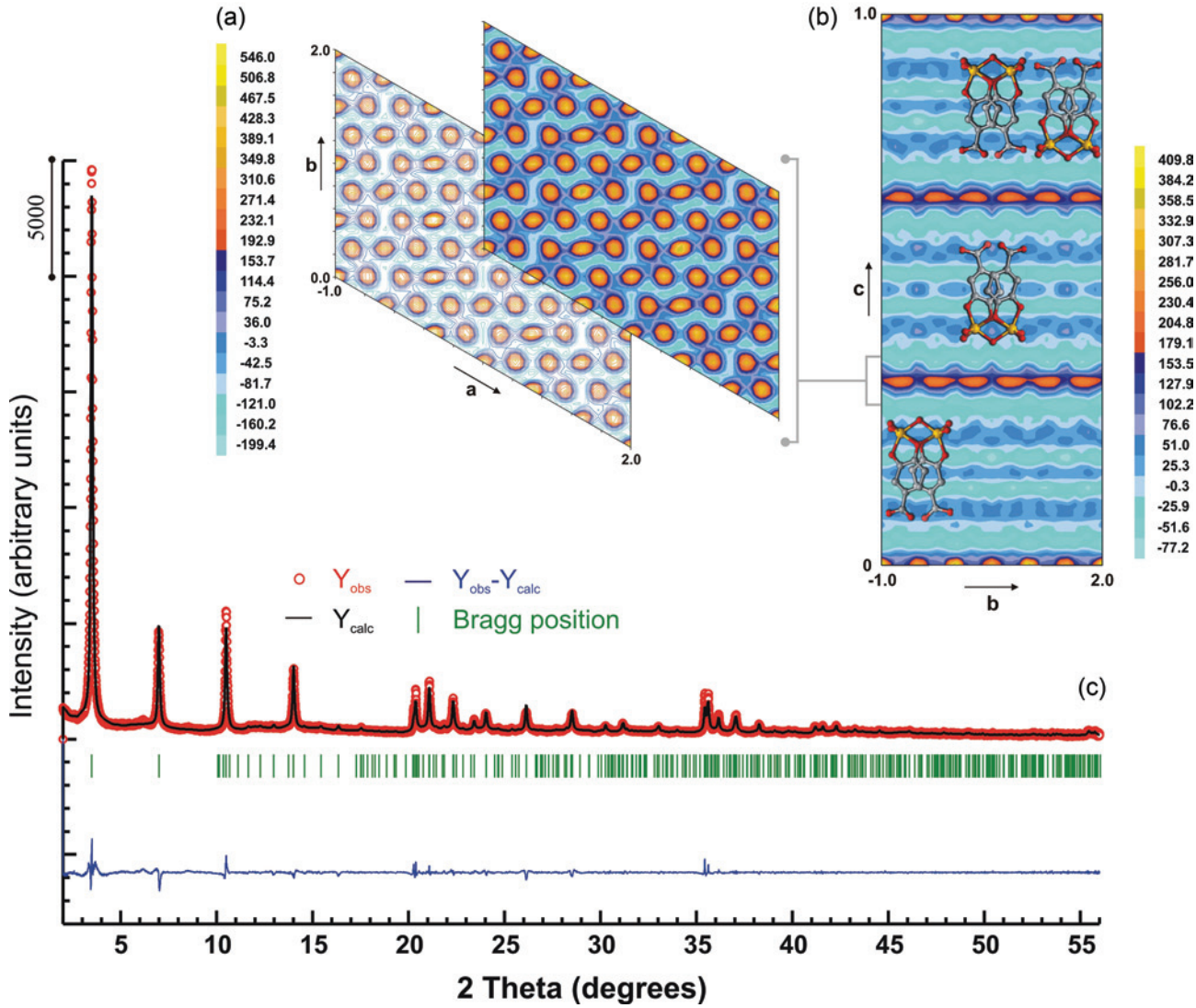

Figure 9. Fourier maps calculated by GFourier and by employing the F_{obs} extracted from a Le Bail whole-powder-diffraction-pattern decomposition of Zn−Al−Mo(50) summed from (a) −0.1 to 0.1 along the *c*-axis, showing the typical hexagonal distribution of $\{AlO_6\}$ and $\{ZnO_6\}$ octahedra in the *ab* plane; (b) 0 to 1 along the *a*-axis, emphasizing the electron density in the interlayer spaces attributed mainly to the presence of disordered $[Mo_2O_5(3,4\text{-dhb})_2]^{m-}$ species (represented in ball-and-stick mode). (c) Experimental data (red circles), Le Bail whole-powder-diffraction-pattern profile fitting (upper solid black line) and difference (lower solid blue line) XRPD pattern. Vertical bars indicate the angular positions of the allowed Bragg reflections for space group $P6_4$ (hexagonal crystal system). Refined unit cell parameters (after Le Bail profile fitting with FullProf.2k): $a = b = 6.1372(1)$ Å, $c = 45.932(2)$ Å; zero point = 0.0017(7)°; $M(16)^{44} = 43.5$ and $F(16)^{45} = 44.2$; Pearson profile function with $M = 1.158(5)$. Caglioti half-width parameters: $U = -0.021(7)$, $V = 0.003(2)$, and $W = 0.0133(2)$. Asymmetry parameters = −0.0042(5) and −0.0015(1). Independent reflections = 603. Global refined parameters = 1. Profile refined parameters = 8. $R_{Bragg} = 0.07\%$ and $\chi^2 = 3.99$.

curves comprising a smooth dehydration step between room temperature and about 225 °C (DTG_{max} = 83 °C), followed by two overlapping weight loss events up to 550 °C (DTG_{max} = 310, 460 °C), leaving a residual mass of 50.4−53.6%. As found for Mg−Al−Mo(50), the Li−Al materials start to lose interlayer water at a lower temperature than that observed for the precursor. The weight loss during the dehydration step increased from about 12% for the samples Li−Al−Mo(*T*)B containing 8.4−9.3 wt % Mo, to about 15% for the samples Li−Al−Mo(*T*)A containing 10.4−11.4 wt % Mo. The 15% weight loss observed for Li−Al−Mo(100)A is slightly lower than the water content of ∼21% calculated for the chemical formula given in Table 2 (with 5 water molecules), which may again be caused bythe presence of strongly held water molecules that are only removed at temperatures above 225 °C.

Conclusions

A series of layered double hydroxides intercalated by oxomolybdenum catecholate complexes have been prepared by ion exchange of precursor materials in nitrate or chloride form. Through a combination of physical methods it was found that dimerization of the monomeric precursor complex (with a Mo/catecholate ratio of 1:2) occurs during contact with the LDH supports, resulting in the cointercalation of $[MoO_2(3,4\text{-dhb})_2]^{m-}$ and $[Mo_2O_5(3,4\text{-dhb})_2]^{m-}$ anions in proportions that depend on the type of LDH support and the reaction conditions. The solution chemistry of Mo^{VI}−cat systems has been well explored, and it is known that in neutral solution the more common *cis*-dioxomolybdenum(VI) species $[MoO_2(cat)_2]^{2-}$ are formed, while in acidic solution, the dimeric $[Mo_2O_5(cat)_2]^{2-}$ anions are observed. Both

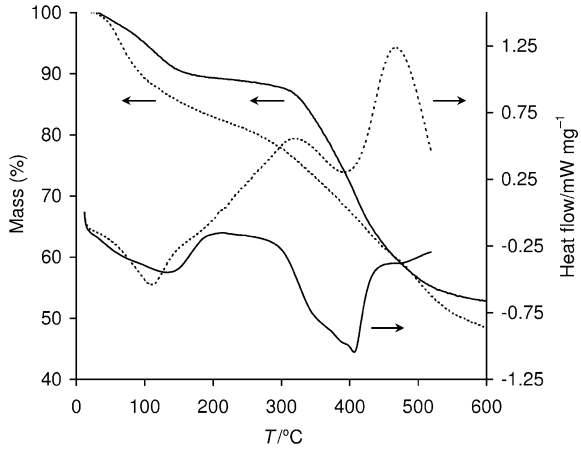

Figure 10. TGA and DSC profiles of Mg−Al−NO_3 (solid lines) and Mg−Al−Mo(50) (dashed lines).

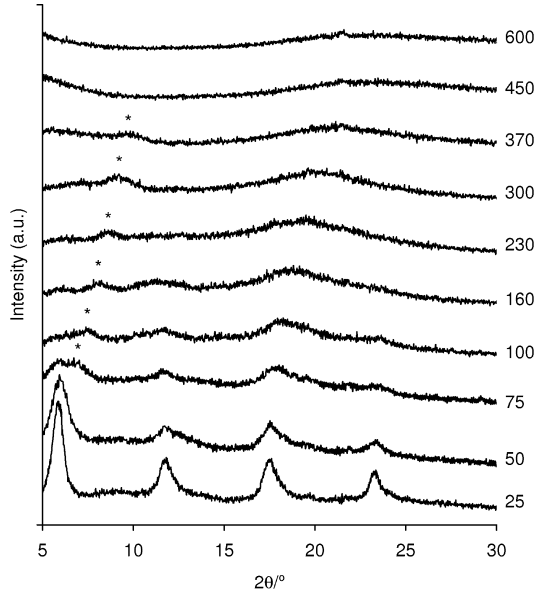

Figure 11. XRPD patterns of Mg−Al−Mo(50) recorded at increasing temperatures in the range 25−600 °C.

species are of interest as possible models of various enzymes.[40] In the preparation of the LDH-Mo^{VI}−cat nanocomposites, the host−guest chemistry seems to influence the solution chemistry of the Mo^{VI}−cat system such that binuclear bis(catecholate) complexes of oxomolybdenum(VI) are formed and intercalated. This was particularly evident for the Zn−Al and Li−Al systems. In the case of the Mg−Al support, the characterization of the final intercalated material indicates that the distribution of different Mo species is weighted toward having more of the monomer. Mg−Al LDHs are more basic than Zn−Al and Li−Al materials, and this may hold back the conversion of the monomer to the dimer. Apparently, in the Li−Al system the monomer can be stabilized for intercalation by carrying out the reaction in a solvent mixture comprising ethanol and water. For the Zn−Al and Li−Al products prepared using only water as solvent, the preferential intercalation of $[Mo_2O_5(3,4\text{-dhb})_2]^{m-}$ species compared with $[MoO_2(3,4\text{-dhb})_2]^{m-}$ may be driven, at least in part, by more favorable host−guest interactions in combination with guest−guest interactions that allow an optimal interlamellar packing arrangement. Indeed, by using the entire reflection data sets extracted from synchrotron X-ray powder diffraction patterns, it was possible to reconstruct electron density maps that not only support the presence of dimeric species in the interlayers but also indicate that these species can adopt an orientation that maximizes the number and geometrical features of the possible hydrogen bonding interactions between the carboxylate and Mo═O groups of the guest and the hydroxyl groups of the host.

Acknowledgment. The authors are grateful to the FCT, OE, and FEDER for financial support (Project POCI//CTM/58507/2004). The CCLRC Daresbury Laboratory Synchrotron Radiation Source (SRS) is acknowledged for providing beamtime at station 16.5 under award number 47105. We also wish to thank the European Synchrotron Radiation Facility (ESRF, Grenoble, France) for granting access to the ID31 high-resolution powder X-ray diffraction beam line and to Dr. Irene Margiolaki for technical assistance. B.M. and S.G. thank the FCT for PhD (SFRH/BD/24717/2005) and postdoctoral (SFRH/BPD/25269/2005) grants, respectively. We also wish to thank Prof. João Rocha for access to research facilities and Luís Mafra for assistance in the NMR experiments.

Supporting Information Available: SEM images and elemental maps for Li−Al−Cl and Zn−Al−Mo(50), conventional XRPD patterns for Zn−Al−NO_3, Zn−Al−Mo(50), and Li−Al−Mo(50)A-C, synchrotron XRPD, Le Bail profile matching, refined unit cell parameters and reconstructed Fourier maps for Li−Al−Cl, Li−Al−Mo(50)A and Li−Al−Mo(100)A, Mo K-edge k^3-weighted EXAFS and Fourier transforms, diffuse reflectance UV−vis spectra, ^{1}H NMR spectrum of the solution recovered after the deintercalation experiment, and TG curves of Li−Al−Cl and Li−Al−Mo(100)A. This material is available free of charge via the Internet at http://pubs.acs.org.

IC800420A